Thermo-mechanical Forming of Al–Mg–Si Alloys: Modeling and Experiments

S. Kurukuri[*,†], A.H. van den Boogaard[†], M. Ghosh[*,**] and A. Miroux[*,**]

[*]*Materials Innovation Institute, P.O. Box 5008, 2600 GA Delft, The Netherlands*
[†]*University of Twente, Faculty of Engineering Technology, P.O. Box 217, 7500 AE Enschede, The Netherlands*
[**]*Delft University of Technology, Faculty of 3mE, P.O. Box 5025, 2600 GA Delft, The Netherlands*

Abstract. In an ongoing quest to realize lighter vehicles with improved fuel efficiency, deformation characteristics of the material AA 6016 is investigated. In the first part of this study, material behavior of Al–Mg–Si sheet alloy is investigated under different process (temperature and strain rate) and loading (uniaxial and biaxial) conditions experimentally. Later, warm cylindrical cup deep drawing experiments were performed to study the effect of various parameters on warm forming processes, such as the effect of punch velocity, holding time, temper and temperature on force-displacement response. The plastic anisotropy of the material which can be directly reflected by the earing behavior of the drawn cups has also been studied. Finite element simulations can be a powerful tool for the design of warm forming processes and tooling. Their accuracy will depend on the availability of material models that are capable of describing the influence of temperature and strain rate on the flow stresses. The physically based Nes model is used to describe the influence of temperature and strain rate and the Vegter yield criterion is used to describe the plastic anisotropy of the sheet. Experimental drawing test data are used to validate the modeling approaches.

Keywords: warm forming, aluminum, deep drawing, earing, simulation, material model
PACS: 81.40.Lm, 81.20.Hy, 46.15.-x, 62.20.fq

INTRODUCTION

Cost effective lightweight vehicles have recently turned out to be a key objective for automotive manufactures due to increasing concerns about reducing environmental impact and improving fuel economy without forfeiting the vehicle performance and comfort. The excellent high strength to weight ratio, good corrosion resistance and recycling potential offered by Al–Mg–Si alloys makes it a good important candidate material to be used in automotive industry. The high alloy percentages in aluminum however, lead to a relatively low room temperature formability compared to mild steel [1]. A promising approach for the improvement of formability is performing the forming processes at elevated temperatures up to the recrystallization temperature. In this process, parts of the tools are heated and other parts are cooled which make it possible to manipulate local flow behavior, in order to increase the formability [2, 3]. However, experience with temperature controlled forming processes is lacking and numerical models are beneficial in optimizing the forming processes. Particularly for warm forming simulations, an accurate coupled thermo-mechanical material model for the anisotropic yield function with temperature and strain rate dependent hardening is required [4, 5, 6].

In this study, our objectives were to: (1) Characterize the material behavior under warm forming conditions *i.e.* uniaxial and biaxial tests were performed to quantify the work hardening and anisotropy of the investigated alloy sheet with change of temperature (2) Experimentally understand and quantify the effects of process parameters such as the effect of temperature, punch velocity, holding time, friction and the effect of tempering on the deep drawing of cylindrical cups by measuring the punch force–displacement curves, the thickness distributions and earing profiles. For this purpose, a commonly used Al–Mg–Si alloy AA 6016 was selected for experimentation. (3) Develop finite element models (FEM) to simulate and validate the warm deep drawing processes. For this purpose, the temperature and strain rate sensitive work hardening according to Nes [7] is used. The anisotropic behavior of the sheet during forming is described by the Vegter yield criterion [8].

EXPERIMENTS

The mechanical behavior of an alloy is mainly determined by its chemical composition, grain size, texture and microstructure. The chemical composition of the alloy was given by the manufacturer and is presented in Table 1.

CP1252, *NUMIFORM 2010, Proceedings of the10th International Conference*
edited by F. Barlat, Y. H. Moon, and M.G. Lee

TABLE 1. Chemical composition of the investigated AA 6016-T4.

%Si	%Fe	%Cu	%Mn	%Mg	%Cr	%Other	%Al
1.03	0.25	0.06	0.15	0.42	0.02	<0.15	rem.

The material was cold rolled, solutionized and naturally aged (T4). The final thickness was 1.01mm. Peak aged (T6) temper condition has been made directly from naturally aged (T4) sheet material by heating at 150 °C for four hours followed by 170 °C for four hours in an oil bath and quenched in water. The as-received material has a cube texture with grain size of 17 μm to 25 μm calculated from XRD measurements.

Uniaxial Tensile Tests

The uniaxial test results are typically important in estimating various parameters that influence formability such as work hardening, anisotropy *etc*. Uniaxial tensile tests were performed at temperatures of 25 °C, 150 °C and 250 °C at strain rates of 0.01 and 0.1 s^{-1}. For every combination of temperature and strain rate at different tempering conditions, one representative stress–strain curve for AA 6016 alloy is shown in Fig. 1.

From Fig. 1, it is clearly seen that the T6 material is stronger compared to T4, at any strain rate and temperature. The main reason for the difference in strength between tempers is due to the different sizes and density of the particles. For the naturally aged temper (T4) many of the particles do not reach the critical size (approximately 5 -10 nm) and are sheared by the dislocations. For the artificially aged alloys (T6) the particles should ideally have the optimum contribution of size and density to give the maximum strength. The rate of work hardening is higher for T4 state at all the temperatures. The difference in rate of hardening is very small at room temperature while at 250 °C there is practically no work-hardening effect in the T6 state, appearing like a plateau before it starts necking. It can also be observed from Fig. 1, that the strain rate sensitivity increases with increasing temperature. At 25 °C, almost no effect of strain rate is shown on the work hardening behavior. At higher temperatures, due to the dynamic recovery of dislocations the flow stress increases with increasing strain rate. This increasing flow stress with increase of strain rate is more clearly visible for T6 condition at 250 °C. However, in Fig. 1(a), at 250 °C the lowest strain rate of 0.001s^{-1} presents the highest flow stress and looks unusual. It is mainly due to more time for dynamic precipitation at the slowest strain rate.

Biaxial Tests

Usually in sheet forming processes, the stress state is biaxial and an infinite number of stress states can be defined by means of an infinite number of strain paths to reach such a stress state. However, the material behavior in multiaxial stress states can be quantified experimentally by a limited number of stress or strain states. Hence, in addition to the uniaxial tests, normal compression tests, plane strain tests and simple shear tests were performed. The normal compression test is equivalent to an equi-biaxial tensile test, assuming that the plastic deformation is independent of

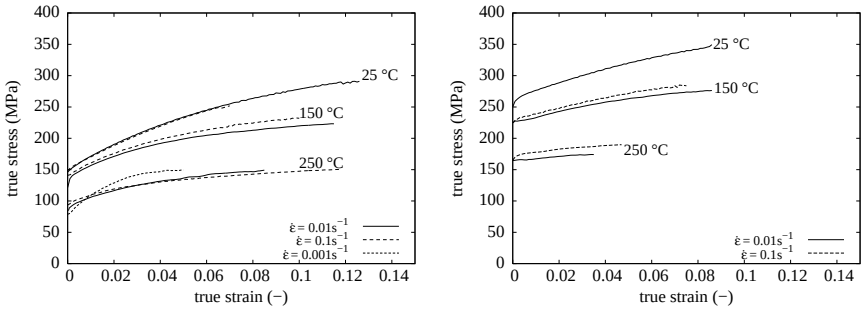

FIGURE 1. Temperature and strain rate influence on true stress–strain curves (a) AA 6016-T4 alloy (b) AA 6016-T6 alloy.

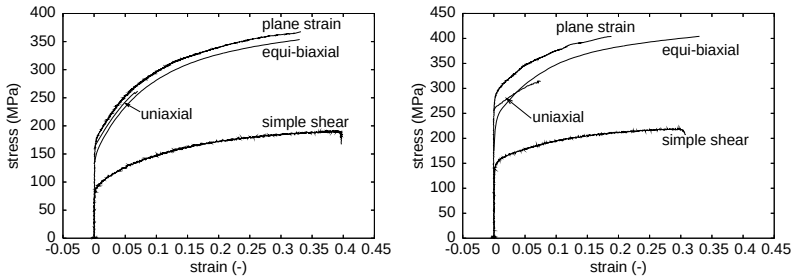

FIGURE 2. Stress–strain curves for different types of loading at room temperature (a) 6016-T4, (b) 6016-T6.

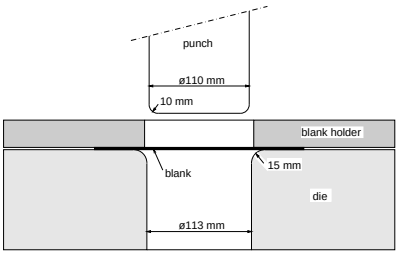

FIGURE 3. Dimensions of the tools for cylindrical cup deep drawing.

the hydrostatic stress. A stack of sheet specimens was prepared with nominal dimensions of $10 \times 10 \times 10$ mm^3. The stack is loaded in the normal direction, and lubricated with oiled PTFE film. The displacement along both in-plane directions is measured using a cross extensometer.

The plane strain tension and simple shear tests were performed using the *Twente biaxial tester*, described by [9] and [10]. In this loading frame a sheet area of 45×3 mm^2 can be deformed in plane strain tension, simple shear or any combination simultaneously. Since, the height of the deformation area is small compared to the thickness the simple shear loading can be applied without material buckling. Also due to the high length to width ratio of the deformation region a plane strain condition at the central region of the deformation area is imposed. However, the edges of the deformation area are free and the deformation state will tend to the uniaxial stress state and this edge effect needs to be taken into account. With these two equipments, no elevated temperature tests can be executed.

Plane strain tension tests were performed with the loading direction perpendicular to the rolling direction and at 45° to the rolling direction. Simple shear tests were performed with the shear direction at $-45°$, 90° and 45° to the rolling direction. For each direction two samples were tested. The stress–strain curves are presented in Fig. 2 together with one uniaxial curve for comparison at two different tempering conditions. These biaxial tests are used to describe the shape of the anisotropic yield locus described in the next sections.

Cylindrical Cup Deep Drawing

Deep drawing is one of the most widely used processes for forming sheet metal parts in automotive industry. It is also a popular process in assessment of formability of sheet metals. In this section, experiments of warm cylindrical cup deep drawing are presented. The objective of these deep drawing tests is to obtain the force–displacement curves during the deep drawing process. After the experiments, the cups were removed and the thickness distribution from the center to the outer diameter in the rolling and transverse direction was measured. Measurement accuracy was found to be ± 0.012mm. Also the earing[1] profile was measured in order to assess the effect of sheet anisotropy in forming operations.

[1] Plastic anisotropy during deep drawing may entail the formation of uneven rims of the drawn product, usually referred to as earing. One important consequence is—besides the irregular shape of the drawn specimen—an inhomogeneous distribution of the mechanical properties and of the wall thickness due to volume conservation.

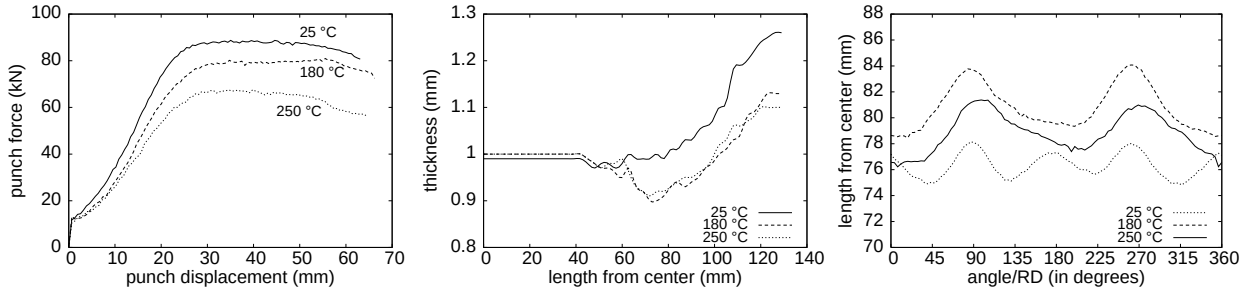

FIGURE 4. Effect of temperature (a) punch force–displacement curves (b) thickness distributions (c) earing profile.

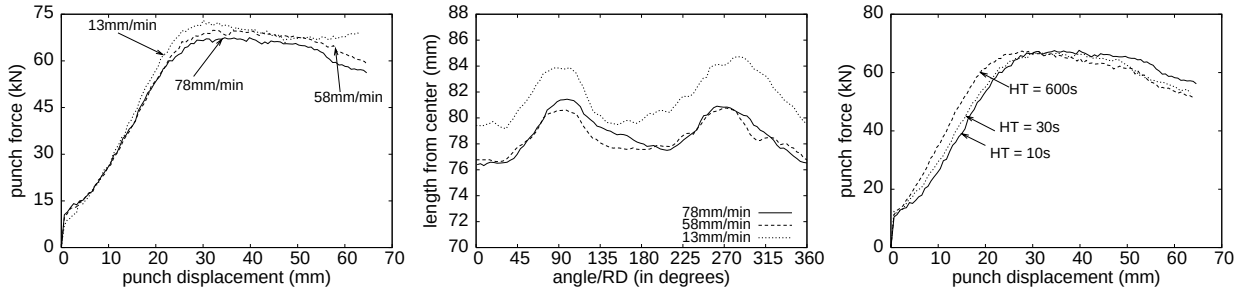

FIGURE 5. Effect of punch velocity (a) & (b) punch force–displacement curves & earing profile; (c) Effect of holding time.

Experiments were performed with a tool set of which the dimensions are given in Fig. 3. All the experiments were performed on blanks of 220 mm diameter that were taken from the same batch of which the uniaxial and biaxial tests were performed. In the experiments, the effective punch stroke was 65 mm. Punch velocities of 13 mm/min to 80 mm/min were used. The die and the blank holder were given a temperature of 25 °C, 180 °C and 250 °C, while the punch was kept at 25 °C. Room temperature drawing tests were done with the blank holding force equal to 90 kN and warm deep drawing tests were done with 54 kN blank holding force.

Effect of Temperature. The effect of temperature is investigated for AA 6016-T4 with a punch velocity of 78 mm/min at 25 °C, 180 °C and 250 °C. From Fig. 4(a), it is clearly seen that with increasing temperature from 25 °C to 250 °C the drawing force decreases significantly. From the thickness distribution along RD presented in Fig. 4(b), it can be seen that the thickness reduction in the wall and flange of the cup is found to be more pronounced at 250 °C compared to room temperature. Figure 4(c) shows that at 25 °C, the earing profile has maxima along RD and TD and minima along 45 ° directions. At higher temperatures AA 6016 shows a minimum along the RD.

Effect of Punch Velocity. The effect of punch velocity is investigated for AA 6016-T4 at 250 °C. The punch velocity was varied from 13 mm/min to 78 mm/min. With lower punch velocity there will be more time for dynamic precipitation leading to stronger response of the material and this fact corresponds with the results obtained (see Fig. 5(a)). However, the effect of precipitation is small compared to other parameters, *e.g.* temperature. Punch velocity seems to have no effect on earing behavior as the nature of the curves for all three velocities are the same. The difference in magnitude of the earing profile for the punch velocity of 13 mm/min is due to a slightly lower drawing depth (63 mm) than the other two velocities (65 mm).

Effect of Holding Time. The effect of holding time was investigated for AA 6016-T4 by holding the blank at 250 °C for different time span before drawing. The punch velocity and blank holding pressure are remain constant. The holding time was varied from 10 s to 600 s. From Fig. 5(c), it is clearly seen that the effect of precipitates is very limited as there is not so much difference among the punch force–displacement curves of different holding times. Although, for longer holding time the punch force–displacement curve is steeper, interestingly the maximum punch force for all the holding times has been found to be the same.

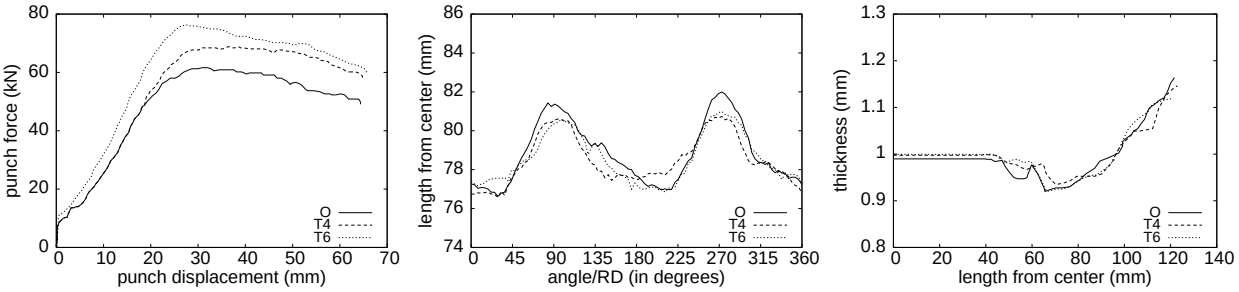

FIGURE 6. Effect of temper (a) punch force–displacement curves (b) thickness distributions (c) earing profile.

Effect of Temper. The punch force–displacement curve at 250 °C presented in Fig. 6(a) shows that the response of T4 and "O" (fully annealed) at the beginning of deformation are equal before T4 gets stronger and deviates after some point. From the measured thickness distribution presented in Fig. 6(b), more thinning at the bottom of the deep drawn cup made of "O" compared to T4 and T6 is observed but this is within the accuracy limit of the experiment. The earing profiles presented in Fig. 6(c) show almost no effect of precipitates (different tempering conditions). The anisotropy remained constant for all levels of temper conditions and did not bring any change in the number and position of ears.

Change of Anisotropy in Deep Drawing at Elevated Temperatures

When cylindrical cup deep drawing is performed on circular blanks, it causes an uneven cup rim (*i.e.* a number of high points called *ears* and an equal number of low points known as *toughs*) as a result of of directional properties or anisotropy of the blank. The effect of anisotropy in deep drawing is generally viewed based on the number of ears, their location with respect to rolling direction and their amplitude. In the previous section, it was clearly seen at room temperature the earing profile exhibits four ears in RD and TD and toughs at 45 ° with similar amplitude in their respective directions. Whereas at elevated temperatures, the earing profile exhibits two ears at TD and toughs close to RD positions.

In order to understand the possible reasons for change of earing profiles from four ears to two ears with the increase of temperature, further analysis was carried out in terms of the effect of orientation of the blank with respect to the reference axis of the tool. Few tests were also conducted to study the effect of friction between the tools and the blank at elevated temperature.

In addition to the series of deep drawing tests presented in the previous section (hereafter called series A), two extra series of deep drawing tests (namely, series B and series C) were performed in order to be more conclusive about the earing or anisotropy behavior based on the punch force–displacement and earing profile measurements. The series B and series C deep drawing tests on AA 6016-T4 alloy were performed by keeping as much similar process parameters as possible in series A. Series B and series C tests were performed 4 years later than the series A tests. A very important note here is that the press tool was rebuilt before performing each series of tests, *i.e.* the orientation of press tool was really different (unknown) between series of tests. It is also pointed out that, unless stated otherwise, all the deep drawing results of Al–Mg–Si alloys presented in this work are from series A.

Effect of Tool Orientation. In this section, the effect of tool orientation is studied by placing the rolling direction of the blank in three different directions *i.e.* 0 °, 90 ° and an arbitrary direction 35 ° to a reference axis of the tool. In Fig. 7, the earing profiles from different series of tests at 25 °C and 250 °C are compared. The earing profile of the cups deep drawn at room temperature exhibit four ears with ears at RD and TD and toughs at $\pm 45°$ from the RD. It shows absolutely no effect of tool orientation on earing behavior (see Fig. 7(a)). At 250 °C, series B tests show not so well defined earing profiles and approximately shows four ears along RD and TD. But, on the other hand, the height of the ears are reduced considerably making the material to be more isotropic at elevated temperature.

Effect of Friction. Effect of friction was studied by varying the amount of lubrication. In these tests of series C, the first two tests were performed with the normal application of the water based lubricant on both sides of the blank. For the next test, the tools were cleaned in order to avoid the lubricant left overs on the tools from previous tests and regular amount of lubricant was applied on the blank. For the last test excess amount of lubricant was applied on both

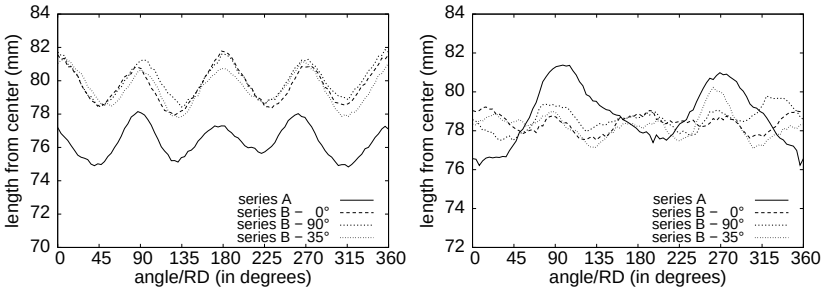

FIGURE 7. Effect of tool orientation on earing profiles (a) at 25 °C (b) at 250 °C.

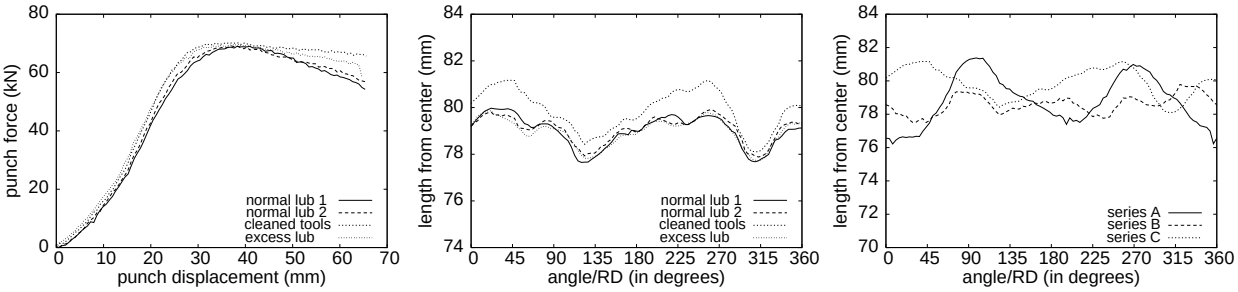

FIGURE 8. (a) & (b) Effect of Friction—punch force–displacement curves & earing profiles. (c) Earing profiles from different series of experiments.

sides of the blank. From the punch force–displacement curves presented in Fig. 8(a), tests with normal application of lubricant are well reproducible. With the tools cleaned before doing a test, the punch force is larger, especially at larger drawing depths. In the test with extra lubricant, the punch force is larger than the test with normal application of the lubricant, this was not expected. From the earing profile plot in Fig. 8(b), it is clearly seen that the results are well reproducible and lubrication conditions do not have an effect on the earing profile, but the height of the ears are dependent on lubrication conditions. When comparing the earing profiles from different series of experiments (see Fig. 8(c)), they are completely different from each other, even though the height of the ears are small for series B and C. It is reminded here that the press tool was rebuilt for each series of tests and it can be concluded that the earing behavior at elevated temperature is highly sensitive to the press tool setup.

FINITE ELEMENT MODELING

The accuracy of finite element simulation of warm aluminum sheet forming will greatly depend on the models that describe the influence of temperature and strain rate on the flow stress, which are governed by the underlying processes such as dislocation evolution to describe the plastic flow. In these models, the hardening process is considered as a competition between dislocation accumulation and the loss of dislocation line length (*i.e.* dynamic recovery). In this study, such a physically based strain hardening "Nes model" [7] is tested for the AA 6016 alloy, which is discussed only briefly in this paper. More details on parameter prediction, which follow from tensile tests, are presented in [6].

The model approach relies on a multi parameter description for the microstructure evolution. At small strains the stored dislocations are arranged in a cell structure characterized by the cell size, δ and the dislocation density within the cells ρ_{i}. At large strains the dynamic recovery of dislocation becomes important and the cell walls collapse into sub-boundaries of well defined misorientations, φ. The microstructure evolution is covered by the following three differential equations:

$$\frac{\mathrm{d}\rho_{\mathrm{i}}}{\mathrm{d}\gamma} = \frac{1}{1+f\left(q_{\mathrm{b}}^2-1\right)} - \frac{\rho_{\mathrm{i}} v}{\dot{\gamma}}, \qquad \frac{\mathrm{d}\delta}{\mathrm{d}\gamma} = -\frac{2\delta^2\rho_{\mathrm{i}}}{\kappa_0\varphi}\frac{SC\rho_{\mathrm{i}}^{-1/2}}{L_{\mathrm{eff}}} + \frac{b\nu_\delta}{\dot{\gamma}}, \qquad \frac{\mathrm{d}\varphi}{\mathrm{d}\gamma} = g(\rho_{\mathrm{i}},\delta,\varphi) \tag{1}$$

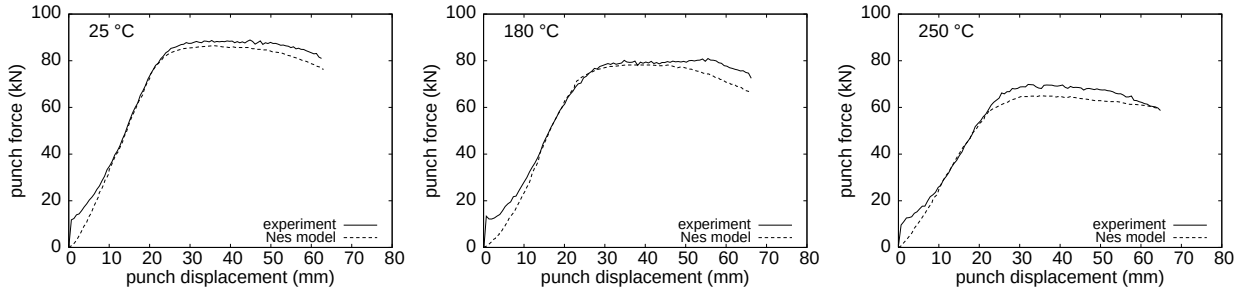

FIGURE 9. Deep drawing of cylindrical cup—experiments and simulations (punch force–displacement curves).

The first term in these equations represents storage of dislocations (which increases work hardening), the second term represents dynamic recovery by annihilation of dislocations (which decreases work hardening). It describes the flow stress as a function of microstructure evolution parameters

$$\tau = \tau_{\mathrm{t}} + \tau_{\mathrm{p}} + \alpha_1 Gb \left[\Gamma_1 \left(\frac{q_{\mathrm{c}}}{\delta \sqrt{\rho_{\mathrm{i}}}} \right) \sqrt{\rho_{\mathrm{i}}} + \Gamma_2 \left(\frac{q_{\mathrm{c}}}{\delta \sqrt{\rho_{\mathrm{i}}}} \right) \frac{q_{\mathrm{c}}}{\delta} \right] + \hat{\alpha}_2 Gb \left[\Gamma_2 (0) \frac{1}{\delta} + \frac{1}{D} \right] \tag{2}$$

Here, τ_{t} is friction or thermal stress, due to short range interactions between mobile dislocations and intersecting stored ones, dragging of jogs, and elements in solid solution. τ_{p} is due to non-shearable particles and the remaining part of the equation represents the long range interaction of the dislocations due to microstructure evolution. Extensive presentations of the microstructure evolution are given in [7]. It is noted that, in this work the flow stress of the Nes model is phenomenologically adapted with the following equation, to describe the higher initial yield strength in T6 condition due to the optimum contribution of size and density of particles.

$$\tau_{\mathrm{T6}} = \tau + 96.5023 + 0.2138 \cdot T - 1.1224 \cdot 10^{-04} \cdot T^2 \tag{3}$$

For the description of the yield surface the Vegter criterion [8] is applied. The Vegter yield criterion is one of the most accurate yield functions for aluminum alloy sheets defined in plane stress conditions. The Vegter yield locus is constructed in principal stress space and uses the Bezier interpolation to connect the measured yield stresses in equi-biaxial, plane strain tension, uniaxial tensile and pure shear tests presented in the previous sections on material characterization. For every part of the yield locus between the two reference stress states, $\vec{\sigma}_i$ and $\vec{\sigma}_j$, a second order Bezier function is determined and the hinge point $\vec{\sigma}_h$ is defined with the tangents drawn at the two reference stress states. The yield locus between the two reference states is defined by:

$$\vec{\sigma}_{\mathrm{locus}} = \vec{\sigma}_i + 2\mu \left(\vec{\sigma}_h - \vec{\sigma}_i \right) + \mu^2 \left(\vec{\sigma}_i + \vec{\sigma}_j - 2\vec{\sigma}_h \right) \qquad \mu \in [0,1] \tag{4}$$

Planar anisotropic behavior can be modeled by defining all reference stress points and corresponding normals depend on the angle θ. The reference stress points and normals are defined by an interpolation, based on Fourier series.

Warm deep drawing simulations of cylindrical cups made up of AA 6016 sheet for different tempering conditions and temperatures are performed with the Vegter and Nes models implemented in the in-house implicit FE code DIEKA. Orthotropic symmetry was assumed for the material model. A quarter of the blank was modeled and boundary conditions were applied on the displacement degrees of freedom to represent the symmetry. The sheets were modeled with 998 discrete Kirchhoff triangular shell elements with 3 translational, 3 rotational and 1 temperature degree of freedom per node. The tools were modeled as rigid contours with a prescribed temperature. In the presented simulations the die and the blank holder were given temperatures of 25 °C, 180 °C and 250 °C, while the punch was kept at 25 °C. In the simulations a temperature dependent friction coefficient is used, with a linear relation from 0.06 to 0.12 for temperatures from 90 °C to 110 °C and constant before and after this range.

In Fig. 9 and Fig. 10, the force–displacement diagrams of the punch and the thickness distributions of the cylindrical cup made of AA 6016-T4 alloy at 64 mm punch displacement/drawing depth are plotted for the experiments and the simulations with the Nes model at different temperatures. Comparing the different punch force–displacement curves, it can be seen that the numerical model underestimates the maximum punch force. The underestimation is slightly higher at 250 °C. At room temperature, the numerical model predicts more thinning at the bottom than observed in the experiments. At elevated temperature, it can be observed that the predicted thickness reduction is slightly better than

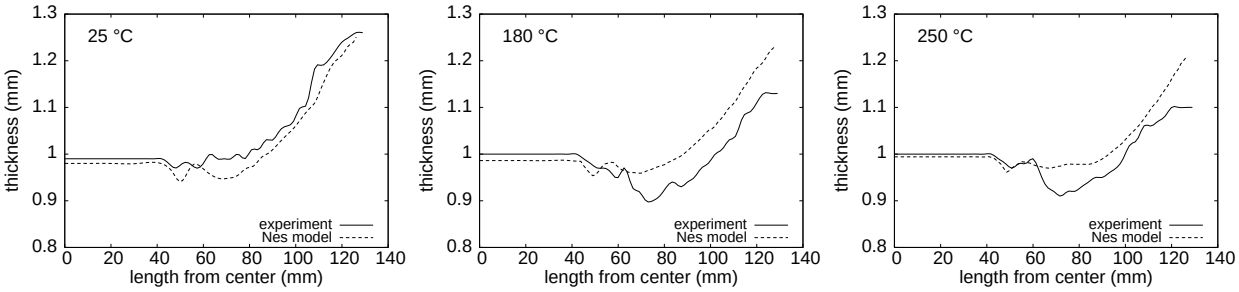

FIGURE 10. Deep drawing of cylindrical cup—experiments and simulations (thickness distribution curves).

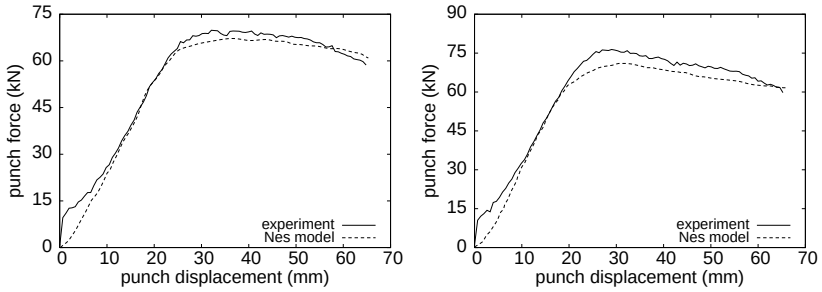

FIGURE 11. Effect of tempering in deep drawing—experiments and simulations (a) 6016-T4 (b) 6016-T6 at 250 °C.

predicted at room temperature. This can be related to the lower punch force predicted by the Nes model. Nevertheless, the numerical model predicted the trends with changing temperature very well.

In Fig. 11, the force–displacement diagrams of the punch are plotted for the simulations and the experiments performed on AA 6016 alloy at different tempering conditions. From the punch force–displacement curves, it can be seen that the numerical model underestimates the maximum punch force for T6 tempering condition more than in T4 condition. It is noted that the higher initial strength in peak aged (T6) condition caused by the precipitates sheared with the moving dislocations is included in the model by a phenomenological fit function given in Eq. (3).

ACKNOWLEDGMENTS

This research was carried out under project number MC1.02106 in the framework of the Research Program of the Materials innovation institute M2i (www.m2i.nl), the former Netherlands Institute for Metals Research. The authors are indebted to P. J. Bolt and R. Werkhoven of TNO Science & Industry for performing the warm deep drawing experiments.

REFERENCES

1. S. Novotny, and M. Geiger, *J. Mat. Proc. Technol.* **138**, 594–599 (2003).
2. F. Shehata, M. J. Painter, and R. Pearce, *J. Mech. Work. Technol.* **2**, 279–291 (1978).
3. P. J. Bolt, N. A. P. M. Lamboo, and P. J. C. M. Rozier, *J. Mat. Proc. Technol.* **115**, 118–221 (2001).
4. A. H. van den Boogaard, and J. Huétink, *Comp. Methods in App. Mech. and Engrg.* **195**, 6691–6709 (2006).
5. N. Abedrabbo, F. Pourboghrat, and J. Carsley, *Int. J. Plast.* **23**, 841–875 (2007).
6. S. Kurukuri, A. H. van den Boogaard, A. Miroux, and B. Holmedal, *J. Mat. Proc. Technol.* **209**, 5636–5645 (2009).
7. E. Nes, *Prog. Mat. Sci.* **145**, 129–193 (1998).
8. H. Vegter, and A. H. van den Boogaard, *Int. J. Plast.* **22**, 557–580 (2006).
9. H. H. Pijlman, *Sheet material characterisation by multi-axial experiments*, Ph.D. thesis, University of Twente (2001).
10. M. van Riel, *Strain path dependency in sheet metal*, Ph.D. thesis, University of Twente (2009).